International Journal of Thermal Sciences 48 (2009) 2036–2045

Contents lists available at ScienceDirect

International Journal of Thermal Sciences

journal homepage: www.elsevier.com/locate/ijts

Flow reversal of laminar mixed convection in the entry region of symmetrically heated, vertical plate channels

Gilles Desrayaud [a,1], Guy Lauriat [b,*]

[a] INSSET, Université de Picardie Jules Verne, Laboratoire Modélisation et Simulation Multi Echelle, MSME FRE 3160 CNRS, 48 rue Raspail, BP 422, F-02109 Saint-Quentin Cedex, France
[b] Université Paris-Est, Laboratoire Modélisation et Simulation Multi Echelle, MSME FRE 3160 CNRS, 5 bd Descartes, F-77454 Marne-la-Vallée Cedex, France

ARTICLE INFO

Article history:
Received 18 September 2008
Received in revised form
8 March 2009
Accepted 8 March 2009
Available online 5 April 2009

Keywords:
Vertical channel
Mixed convection
Flow reversal
Numerical heat transfer

ABSTRACT

The present numerical investigation is concerned with flow reversal phenomena for laminar, mixed convection of air in a vertical parallel-plate channel of finite length. Results are obtained for buoyancy-assisted flow in a symmetrically heated channel with uniform wall temperatures for various Grashof numbers and Reynolds numbers in the range $300 \leq Re \leq 1300$. The effects of buoyancy forces on the flow pattern are investigated and the shapes of velocity and temperature profiles are discussed in detail. Flow reversals centred in the entrance of the channel are predicted. The strength of the cells decreases as the Reynolds number is increased, until they disappear. The regime of reversed flow is identified for high values of the Péclet number in a Pe–Gr/Re map. It is also shown that the channel length has no influence on the occurrence of the reversal flow provided that $H/D \geq 10$.

1. Introduction

Combined free and forced convection in vertical heated pipes has received considerable attention because of their practical industrial and engineering applications, such as electronic equipment, solar systems, nuclear reactors, heat exchangers and chemical processes. Because of practical interest, numerous investigations of mixed flows in vertical heated pipes have been conducted analytically, numerically and experimentally by various researchers (see for instance the comprehensive review of Jackson et al. [1]).

Hanratty et al. [2], Scheele and Hanratty [3] were among the first to present both analytical and experimental observations revealing the existence of flow reversal in the fully developed region at low Reynolds number for buoyancy-assisted flow in circular tubes. The fluid in the tube centre is decelerated to such an extent that the flow is reversed. Far enough downstream, this inverted flow becomes unstable and a region of turbulent flow is obtained. Zeldin and Schmidt [4] carried out a numerical study of this developing mixed-convection flow in a vertical isothermal tube, taking into account the axial diffusion of heat and momentum; *i.e.*, the full elliptic equations. They considered two different hydrodynamic entrance conditions: uniform irrotational, and fully developed velocity entrance models, both with uniform entrance temperature. The former model agreed fairly well with experimental results, the velocity profiles exhibiting some central concavity near the tube entrance region but with no evidence of recirculation cells. Yao [5] studied the stability of a fully developed upward flow in a heated vertical pipe (with linear wall temperature distribution) and demonstrated that the mixed flow is highly unstable, the instability being supercritical. The disturbed flow has a double-spiral structure. Morton et al. [6] and Ingham et al. [7] performed experimental and numerical investigations for the situations of steady recirculating mixed-convection water flows in vertical circular tubes for relatively small Reynolds number. Bernier and Baliga [8,9], using a technique which allows direct visualization of fluid flow-phenomena, observed the presence of recirculation cells and also of laminar-turbulent transitions at low values of the Reynolds number for fully developed flow in a closed-loop thermosyphon with uniform heat flux boundary condition. Wang et al. [10] in a numerical study of fully developed flow in horizontal (3D study) and vertical (axially symmetric 2D flow) pipes investigated the effect of axial conduction and identified the regime of reversed flow occurrence for various Prandtl numbers in the Pe–Gr/Re coordinates. Moutsoglou and Kwon [11] numerically studied developing flow in vertical tubes for both assisting and opposing laminar mixed convection and solved the parabolised equations with uniform temperature or heat flux boundary conditions. They determined the critical buoyancy parameter, Gr/Re, that indicates

* Corresponding author. Tel.: +33 1 60 95 72 69; fax: +33 1 60 95 72 94.
E-mail address: lauriat@univ-mlv.fr (G. Lauriat).
[1] Deceased on January 28th, 2009.

1290-0729/$ – see front matter © 2009 Elsevier Masson SAS. All rights reserved.
doi:10.1016/j.ijthermalsci.2009.03.002

Nomenclature

A	aspect ratio of the channel (H/D)
D	width of the channel, m
f	local Fanning friction factor
$\overline{f}$	overall Fanning friction factor
g	gravitational acceleration, m s^{-2}
Gr	Grashof number, $g\beta\,(T_w - T_0)D^3/\nu^2$
H	height of the channel, m
Nu	local Nusselt number
$\overline{\mathrm{Nu}}$	overall Nusselt number
N_x, N_y	number of cells in the X and Y-direction
P_m	dimensionless motion pressure
Pe	Péclet number, Re Pr
Pr	Prandtl number, ν/α
Re	Reynolds number, $(2D)u_0/\nu$
Ri	Richardson number, Gr/Re^2
T	dimensional temperature, K
T_0	inlet temperature, K
T_b	dimensional bulk temperature, K
T_w	dimensional wall temperature, K
u_0	dimensional mean velocity, m s^{-1}
X	dimensionless streamwise coordinate, x/D
Y	dimensionless transverse coordinate, y/D
U, V	dimensionless velocity components in X and Y directions

Greek symbols

α	thermal diffusivity of the fluid, m^2 s^{-1}
β	thermal expansion coefficient of fluid, K^{-1}
ν	kinematic viscosity of fluid, m^2 s^{-1}
ρ	density, kg m^{-3}
θ	dimensionless temperature

the onset of flow reversal. However, they were only able to detect this onset because they used a parabolic formulation of the governing equations. Nesreddine et al. [12], in a numerical study of fully developed upward and downward laminar mixed convection of air in a vertical tube with a short uniformly heated section, showed that axial diffusions of momentum and heat can significantly influence the hydrodynamic and thermal fields. This work was extended for developing flow regions by Zghal et al. [13] but without finding any reversed flow.

The majority of the studies have dealt with pipes of circular section, and few papers are devoted to parallel-plate vertical channels with various kinds of boundary conditions to examine reversed flow occurrence. Aung and Worku [14] analytically demonstrated that reversed flow is impossible in the case of fully developed flow for symmetrically heated channels at constant temperature. Cheng et al. [15] presented some analytical solutions of the fully developed laminar combined free and forced convection in vertical parallel-plate channels under various thermal boundary conditions: isoflux–isoflux, isoflux–isothermal, and isothermal–isothermal. Based on their theoretical solutions, reversed flow zones were obtained for different heating conditions on walls; their findings confirmed the conclusions presented by Aung and Worku [14] that, in fully developed flow, no bidirectional flow is possible in a duct in which the walls are at an identical temperature. Linear stability analysis of laminar mixed convection in a vertical channel with constant heat flux imposed on the walls has been investigated by Chen and Chung [16]. They demonstrated that the fully developed flow is highly unstable, the critical Grashof number being strongly dependent on the Reynolds and Prandtl numbers. Nonlinear local analysis [17] gave results in good agreement with those of Chen and Chung [16].

In the developing flow region, Habchi and Acharya [18] using the boundary-layer assumptions numerically solved parabolic equations by a marching method for symmetrically or asymmetrically heated vertical parallel-plate channels at uniform temperature. They failed numerically to find reversed flow in the developing flow region as Aung and Worku [19]. Ingham et al. [20,21] conducted numerical investigations using a marching technique into developing laminar mixed flows in vertical parallel ducts with symmetric and asymmetric constant wall temperature boundary conditions. They studied situations where heating in upflow (or cooling in downflow) causes reversed flow to occur at the centre of the duct, and situations where cooling in upflow (or heating in downflow) causes reversed flow to occur adjacent to the wall. Ingham et al. [20] found flow reversal near the centre of a parallel-plate duct with symmetric wall temperature boundary conditions for two values of the Gr/Re parameter, 350 and 600. Azizi et al. [22] in a recent numerical study only showed recirculation occurrence in the case of opposing flow (*i.e.*, along the walls) but they examined only a few particular cases. Some attempts at numerical simulations of flow reversal in the entrance region of a rectangular duct have been reported by Cheng et al. [23] but no reversed flow in the centre part of the duct was put in evidence.

The purpose of the present paper is to examine the upward mixed-convection heat transfer behaviour in vertical channels with symmetric constant wall temperature boundary conditions in order to clarify the conditions under which, in developing flow regions, reversed flow does occur. This is achieved by numerically solving the elliptic governing equations in the case of aiding buoyancy force.

2. Governing equations and numerical method

The physical model under consideration (Fig. 1) consists of a two-dimensional channel of width D. Channel walls are maintained at a temperature T_w greater than the temperature T_0 of the inlet fluid. The working fluid is taken to be air and the flow is assumed to be incompressible, laminar and two-dimensional, and viscous dissipation is negligible. The fluid properties are assumed to be constant except for the variation of the density in the buoyancy term of the momentum equation (Boussinesq approximation).

The governing equations and boundary conditions are expressed in dimensionless form as follows:

Conservation of mass

$$\frac{\partial U}{\partial X} + \frac{\partial V}{\partial Y} = 0 \tag{1}$$

Conservation of momentum

$$\frac{\partial (UU)}{\partial X} + \frac{\partial (VU)}{\partial Y} = -\frac{\partial P_m}{\partial X} + \frac{2}{Re}\left(\frac{\partial^2 U}{\partial X^2} + \frac{\partial^2 U}{\partial Y^2}\right) + \frac{4Gr}{Re^2}\theta \tag{2a}$$

$$\frac{\partial (UV)}{\partial X} + \frac{\partial (VV)}{\partial Y} = -\frac{\partial P_m}{\partial Y} + \frac{2}{Re}\left(\frac{\partial^2 V}{\partial X^2} + \frac{\partial^2 V}{\partial Y^2}\right) \tag{2b}$$

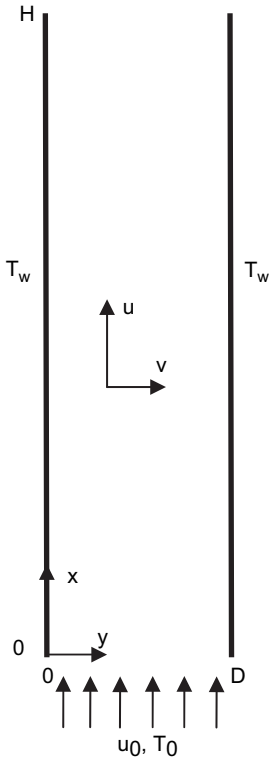

Fig. 1. Calculation domain and dimensional coordinate system of the parallel-plate duct.

Conservation of energy

$$\frac{\partial(U\theta)}{\partial X}+\frac{\partial(V\theta)}{\partial Y}=\frac{2}{Pe}\left(\frac{\partial^2\theta}{\partial X^2}+\frac{\partial^2\theta}{\partial Y^2}\right) \tag{3}$$

where the dimensionless variables are as follows:

$$X=x/D,\quad Y=y/D,\quad U=u/u_0,\quad V=v/u_0,$$
$$P_m=(p+\rho_0 gx)/\rho_0 u_0^2,\quad \theta=(T-T_0)/(T_w-T_0) \tag{4}$$

At the inlet of the channel, the fluid has a uniform vertically upward streamwise velocity distribution,

$$X=0,\quad 0\le Y\le 1\quad U=1,\ V=0,\ \theta=0\ \textit{and}\ \frac{\partial P_m}{\partial X}=0 \tag{5a}$$

Some numerical experiments were made using as inlet velocity the corresponding parabolic velocity profile:

$$U=6Y(1-Y) \tag{5b}$$

i.e., the parabolic velocity profile of fully developed flow.

Boundary conditions of uniform wall temperature are considered and the usual non-slip conditions apply at the channel walls,

$$Y=0\ \textit{and}\ 1,\quad 0\le X\le A\quad U=V=0,\quad \theta=1 \tag{6}$$

At the outlet of the channel, zero streamwise gradient of the variables is considered with specified ambient pressure,

$$X=A,\ 0\le Y\le 1\quad \frac{\partial U}{\partial X}=\frac{\partial V}{\partial X}=\frac{\partial\theta}{\partial X}=0\quad P_m=0 \tag{7}$$

From the governing equations and boundary conditions, the relevant dimensionless parameters of the present problem are the Reynolds number, based on the hydraulic diameter of the channel, the Prandtl and Grashof numbers ($\mathrm{Re}=2Du_0/\nu$, $\mathrm{Pr}=\nu/\alpha$, $\mathrm{Gr}=g\beta(T_w-T_0)D^3/\nu^2$) or the Reynolds number, the Richardson number, $\mathrm{Ri}=\mathrm{Gr}/\mathrm{Re}^2$ (the buoyancy force parameter Gr/Re is also often used), and the Péclet number, $\mathrm{Pe}=\mathrm{Re}\ \mathrm{Pr}$. The aspect ratio of the channel, $A=H/D$, is the only geometrical parameter.

Since the magnitude of the Péclet number used in this paper is always greater than 200, the axial heat conduction from the heated region to the upstream region is considered negligible (Nesreddine et al. [12]). Hence the entry boundary conditions (Eq. (5)) seem reasonable for the range of selected parameters (situated in zone I and III of negligible preheating in Fig. 11a; Nesreddine et al. [12]). This was also confirmed by Zghal et al. [13] who showed that, for these values of the Richardson and Péclet numbers, the temperature profile change compared to a uniform one is lower than 2%, while the velocity profile change compared to the parabolic profile is greater than 2%. It will be demonstrated that the entry velocity profile is of less importance in the present study.

The dimensional bulk temperature is calculated using

$$T_b(x)=\frac{\int_0^D \rho_0 uT\,\mathrm{d}y}{\int_0^D \rho_0 u\,\mathrm{d}y} \tag{8}$$

The local and overall bulk Nusselt numbers are defined as:

$$Nu=\frac{-2}{1-\theta_b}\left.\frac{\partial\theta}{\partial Y}\right|_w\quad \overline{Nu}=\frac{1}{A}\int_0^A Nu\,\mathrm{d}X \tag{9}$$

while the local and average Fanning friction factors are,

$$fRe=2\left.\frac{\partial U}{\partial Y}\right|_w\quad \overline{f}Re=\frac{2}{A}\int_0^A\left.\frac{\partial U}{\partial Y}\right|_w\mathrm{d}X \tag{10}$$

The numerical method used to solve the set of non-linear and coupled partial differential equations presented above is based on the SIMPLE finite volume approach of Patankar [24] recently improved through the IDEAL scheme proposed by Sun et al. [25]. Complete information regarding the numerical method is well documented in the papers by Sun et al. [25,26]. All the conservation equations were cast into a transient form with a semi-implicit scheme for temporal integration (ADI method). All the computational results presented here are thus obtained as stationary asymptotic solutions of transient evolution processes. Grids were chosen to be nonuniform in the axial and transverse directions to account for uneven variations of velocity and temperature at the inlet and outlet of the channel and boundary layers near the walls.

The overall convergence of the IDEAL procedure was determined by using the L2-norm of the variable fields (U, V, θ) between two successive iterations. The solution was considered to have converged when the values of the L2-norm of both components of the velocity and of the temperature are below 10^{-8}. In order to ensure that the results were independent of grid size, computations were carried out for the following conditions: $\mathrm{Re}=300$, $\mathrm{Pr}=0.7$, $A=50$, $\mathrm{Gr}=1.59\times10^5$ (corresponding to $D=0.03$ m). Global (average Fanning friction factor

and average Nusselt number) and local values of the maximum of the axial velocity and temperature on the centreline at position $x_6 = 0.18$ m were compared for various grids. Results in Table 1 suggest that the 200×42 grid is sufficiently fine to give an accurate solution. Contour plots of stream function and temperature distributions for the three finest grids were found to be almost identical. It should be noted that all along the wall, the local bulk Nu number decreases and reaches an asymptotic value as soon as the flow becomes developed and the buoyancy force disappears, which is in agreement with the zero buoyancy fully developed limit of 7.54. Concerning the local Fanning friction factor times the Reynolds number, its value asymptotically reaches the corresponding one for pure forced convection which is equal to 24 for fully developed conditions.

The numerical code was also validated by comparing its predictions with numerical results obtained using other codes, an in-house code based on the SIMPLER algorithm which has been extensively used elsewhere (Desrayaud and Lauriat [27]) and a commercial one, FLUENT (Fluent [28]). Reversed flow predictions were also obtained with these codes (see also the results of Laaroussi et al. [29]). These comparisons confirm the validity of the numerical scheme.

3. Results and discussion

Results are obtained for $\mathrm{Re} = 300$, 500, 1000 and 1300. Even if non-dimensional variables and dimensionless equations are used to solve this problem, some characteristic dimensional quantities are given to avoid unrealistic values, which can occur when using dimensionless numbers without discernment. Thus, the wall temperature has been fixed to $T_w = 60\,^\circ\mathrm{C}$ while the inlet fluid temperature is $T_0 = 10\,^\circ\mathrm{C}$. The working fluid is air and the Prandtl number at the average temperature is equal to $\mathrm{Pr} = 0.7$. The Grashof number ($\mathrm{Gr} = g\ \beta\ (T_w - T_0)\ D^3/\nu^2$) is then varied by varying the width of the channel which is taken to range from $D = 0.02$ m to 0.06 m. This gives a range of the Grashof number from 4.71×10^4 to 1.27×10^6.

In this investigation it has been assumed that the Boussinesq approximation is valid despite the rather high temperature difference of 50 °C. It has been shown recently, in a study of a binary mixture of perfect gases with and without variable thermophysical properties that reversed flow occurs in all of these cases too (Laaroussi et al., Fig. 16, [29]). Since the aim of the present study is to investigate reversed flows in an isothermal channel of finite length, the Boussinesq approximation is used for the sake of simplicity. It should be emphasized that this approximation does not alter the physical mechanism at the origin of the onset of reversed flows.

3.1. Influence of the Grashof number

Previous studies in vertical heated pipes and channels have shown that for ascending heated flow, the effect of natural convection is to accelerate the flow near the walls and to decelerate the flow near the centre of the duct, the magnitude of the distortion of the velocity being dependent upon the Richardson number (or the Gr/Re ratio). This is clearly exemplified in Fig. 2 which shows the dimensionless streamlines at a constant Reynolds number of 300; the aspect ratio of the channel is kept constant, $A = 50$, for various values of the Grashof number, which is varied by changing the width of the channel from $D = 0.02$ to 0.06 m. It should be noted that for reasons of clarity the width and the height of the channel in the pictures are always the same, whatever the real channel dimensions. For $D = 0.02$ m (Fig. 2a), at the channel entrance the streamlines are slightly narrowed, showing an acceleration of the fluid at the walls in this region. The streamlines then become parallel. This indicates that the axial velocity profile is independent of the streamwise direction, at least by the time it reaches the outlet of a sufficiently long channel, and that the flow is fully developed. For $D = 0.025$ m (Fig. 2b), the flow along the two walls accelerates too, and thus two symmetrical recirculation cells associated with flow reversal are engendered in the centre of the channel at the entrance. It should be noted that in the present study a class of mixed convection flows between parallel-plate channels is considered in which the net through-flow rates are constant: at a constant Reynolds number, the mass flow rate is kept constant whatever the Grashof number. Moreover, increasing the Grashof number by increasing the channel width (as is done here) diminishes the average velocity at the channel entrance (*i.e.*, u_0 in the legend of Fig. 2) while the buoyancy force is constant, the inlet and wall temperature always keeping the same values. The inertia force thus decreases as D increases, while the buoyancy force is constant; this explains why, when increasing the Grashof number, the recirculation cells expand in both transverse and axial directions, always starting in the channel entrance where the largest temperature differences exist (see Fig. 6 in the following).

The dimensional thermal fields presented in Fig. 3 correspond to the streamline plots shown in Fig. 2. The interval of isotherms is 5 °C, from 10 °C (inlet temperature) to 60 °C (wall temperature) plus one specific value here, 59 °C. The effects of reversed flow are clearly visible at the channel entrance comparing Fig. 3a (without reversed flow) and Fig. 3b–d (with reversed flow). In the latter cases, the temperature in the centre part of the entrance is uniform, extending in the transverse direction with its magnitude constant when increasing the Grashof number.

Fig. 4a illustrates the development of the dimensional axial velocity profiles for $\mathrm{Re} = 300$ and $\mathrm{Gr} = 1.59 \times 10^5$ ($D = 0.03$ m). At x_6 (equal to 0.18 m in this case), near the entrance, the profile is characterized by a negative velocity core indicating reversed flow, and velocity maximums near the wall to ensure mass conservation. As x is increased to $x_{10} = 0.30$ m, the two symmetrical velocity maximums shift toward the centre, decreasing their strength, and the depressed centreline velocity is less and less marked ($x_{20} = 0.60$ m), finally disappearing, the flow becoming almost fully developed ($x_{45} = 1.35$ m). Fig. 4b shows the streamwise development of the axial dimensional temperature profiles. The reversed flow near the channel entrance makes the fluid temperature more uniform (see x_6 profile) and, ultimately the fluid flow attains an isothermal state. The velocity and temperature profiles at the channel exit approach the fully developed flow conditions, *i.e.*, the parabolic axial velocity (indicated by a dashed line), which is invariant in the direction of flow and the uniform temperature profile of 60 °C.

Fig. 5a, which shows the centreline axial velocity for three different widths of the channel and constant Reynolds number ($\mathrm{Re} = 300$), indicates that the onset of flow reversal depends on the Grashof number, while the dimensional point of flow separation of the recirculation region at the centre of the channel appears to be independent of the Grashof number. The behaviour of the centreline axial velocity in the recirculation cells is quite different to that

Table 1
Comparison of local and average values for various grids. $\mathrm{Re} = 300$, $\mathrm{Pr} = 0.7$, $\mathrm{A} = 50$, $\mathrm{Gr} = 1.59 \times 10^5$ ($D = 0.03$ m).

N_x, N_y	$\overline{\mathrm{Nu}}$	$\overline{f}\,\mathrm{Re}$	$T(x_6, 0.5D)$, °C	$u_{\max}(x_6, y)$, cm s^{-1}
100, 22	10.62	60.28	36.17	17.50
150, 32	10.54	64.50	35.62	17.75
200, 42	10.51	67.05	35.05	18.02
250, 52	10.48	68.00	35.03	18.03
300, 62	10.48	68.08	34.89	18.07

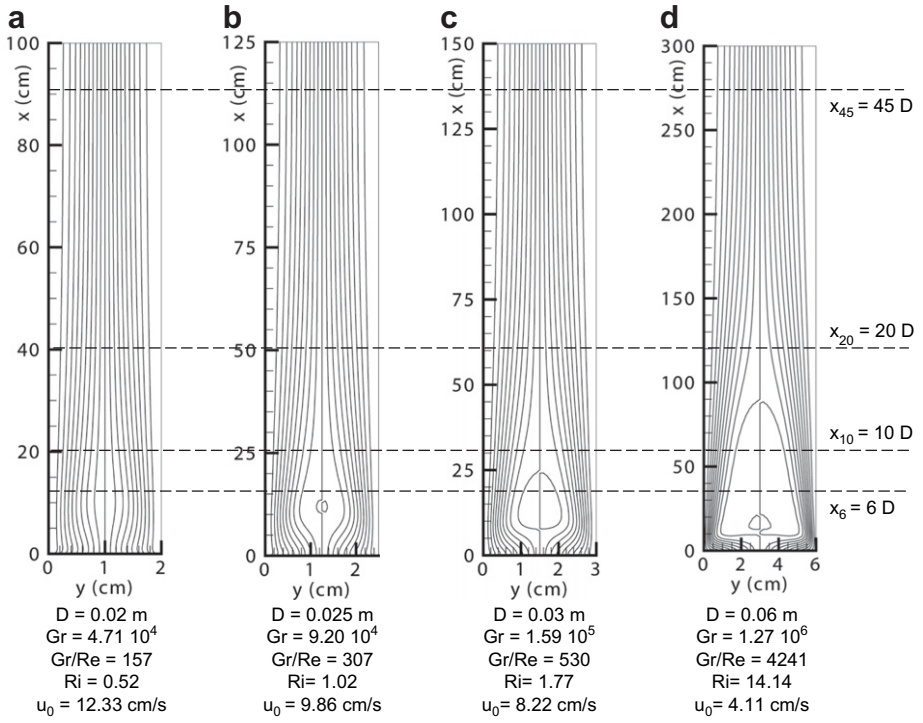

Fig. 2. Streamlines for various widths of the channel at a fixed Reynolds number, Re = 300. Note that the scale of the transverse direction is 10 times the scale of the axial direction. (Isolines: from 0 to 1 by 0.05 step). a) $D = 0.02$ m, $Gr = 4.71 \times 10^4$, $Gr/Re = 157$, $Ri = 0.52$, $u_0 = 12.33$ cm s^{-1}. b) $D = 0.025$ m, $Gr = 9.20 \times 10^4$, $Gr/Re = 307$, $Ri = 1.02$, $u_0 = 9.86$ cm s^{-1}. c) $D = 0.03$ m, $Gr = 1.59 \times 10^5$, $Gr/Re = 530$, $Ri = 1.77$, $u_0 = 8.22$ cm s^{-1}. d) $D = 0.06$ m, $Gr = 1.27 \times 10^6$, $Gr/Re = 4241$, $Ri = 14.14$, $u_0 = 4.11$ cm s^{-1}.

observed in the case of constant heat flux heating. Fig. 5a shows that, while the position of the stagnation point is the same when Gr is increased, the position of the velocity minimum strongly depends on the Gr value, and is always positioned in the axial centre of the recirculation cells. Moreover, the axial velocity increases immediately after reaching its minimum and no region of constant axial velocity inside the recirculation cells has ever been observed for uniform isothermal heating, as was observed by Zghal et al. [13] in the case of uniform heat flux. It should be noted that for this Reynolds number, the channel is long enough for a fully developed region to be reached by the flow. The maximum outlet axial velocity decreases as the channel width increases owing to the constant mass flow rate. Looking at the centreline pressure evolution, Fig. 5b shows that the trend is the same whatever the Grashof

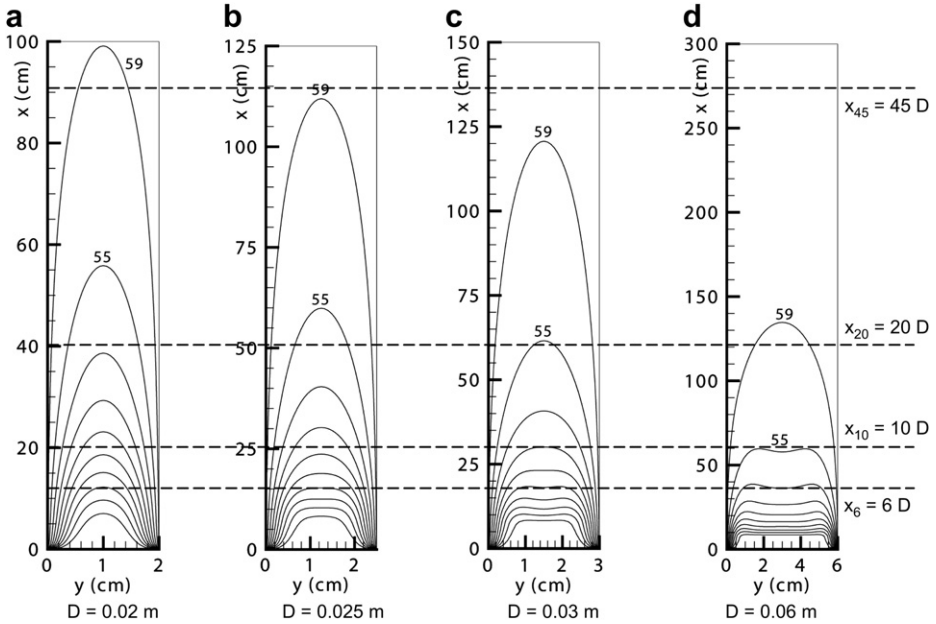

Fig. 3. Thermal fields for various widths of the channel at a fixed Reynolds number, Re = 300 (*Isolines: from 10 °C (inlet) to 60 °C (walls) by 5 °C step + 59 °C*). a) $D = 0.02$ m. b) $D = 0.025$ m. c) $D = 0.03$ m. d) $D = 0.06$ m.

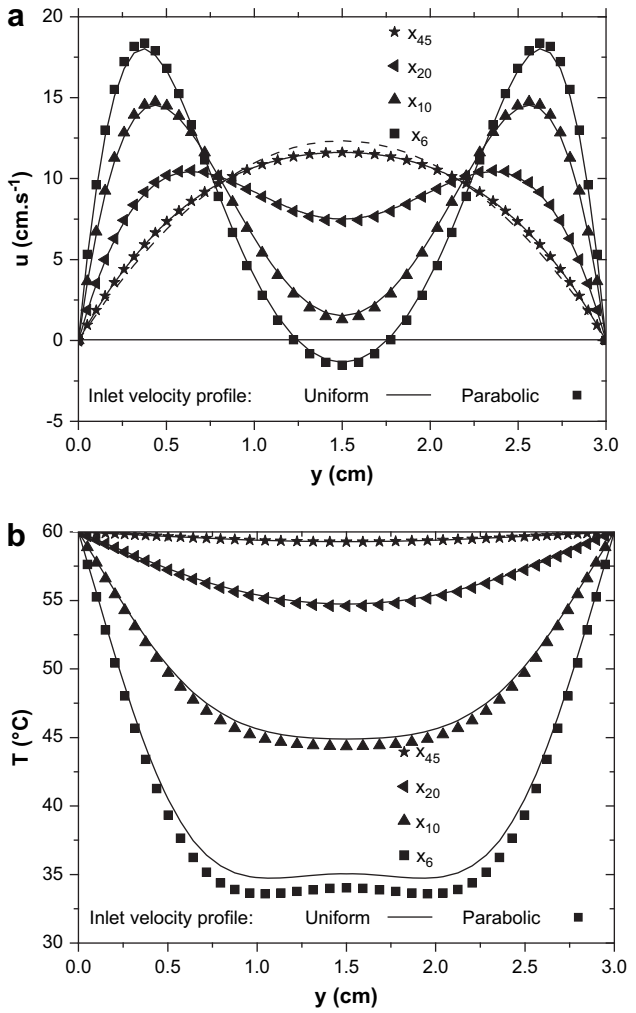

Fig. 4. Streamwise axial velocity profiles (a) and temperature distributions (b) as a function of position and of inlet velocity profile: $x_6 = 0.18$ m, $x_{10} = 0.30$ m, $x_{20} = 0.60$ m, $x_{45} = 1.35$ m. Re = 300, Gr = 1.59×10^5, $A = 50$ ($D = 0.03$ m, $H = 1.50$ m).

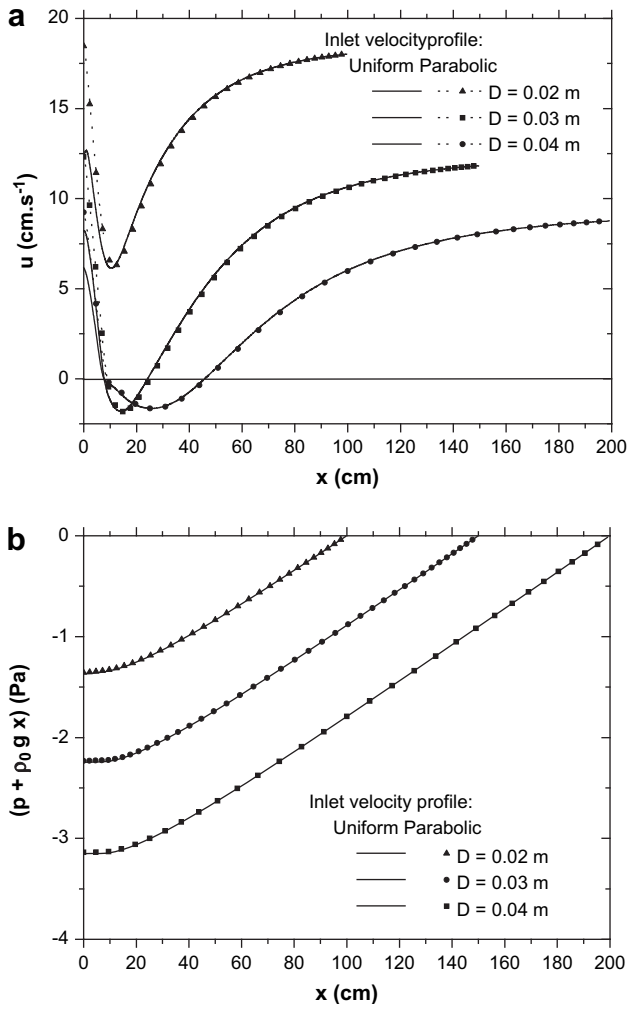

Fig. 5. Streamwise variation of the centreline axial velocity (a) and pressure (b) for various channel widths and for two inlet velocity profiles, Re = 300, $A = 50$.

number, and is not perturbed by the presence of a reversed flow. A horizontal plateau can be seen at the channel entrance followed by a linear increase of the pressure until the outlet is reached, where the pressure defect is zero, *i.e.*, the pressure is ambient pressure.

Contrarily to what was found in the case of uniform heat flux (Zghal et al. [13]), no fully developed region (*i.e.*, axially independent variables) with flow reversal can exist for isothermal heating, the axial velocity on the centreline never being constant inside the flow reversal. Temperature evolution on the centreline in Fig. 6 highlights this behaviour. The axial variation of the dimensional centreline and bulk temperatures is presented in Fig. 6 for Re = 300 and Gr = 1.59×10^5 ($D = 0.03$ m). An examination of Fig. 6 reveals a sharp increase of the temperature of the fluid occurring in the first quarter of the channel (by almost 40 °C), followed by a smooth increase (by only 10 °C) before reaching a value close to the wall temperature. This step rise, which exists without the presence of reversed flow, always occurs even for large channel widths, due to the fact that all of the incoming fluid is then forced to move close to the wall by the recirculation region, thus keeping the heat transfer process always efficient (see Fig. 7). Moreover, a small plateau of constant inlet temperature can be seen at the beginning of the centreline temperature. This behaviour is not due to the recirculation cells because this phenomenon can also be observed in channels without flow reversal. Finally, for these particular parameters, the temperature of the fluid at the outlet of the channel almost reaches the wall temperature, *i.e.*, 60 °C. The axial variation of

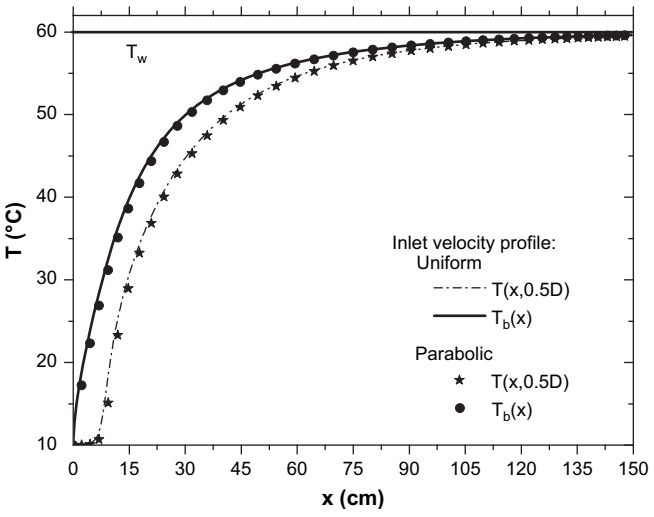

Fig. 6. Streamwise variation of the centreline and bulk temperature, $D = 0.03$ m. Re = 300, Gr = 1.59×10^5, $A = 50$.

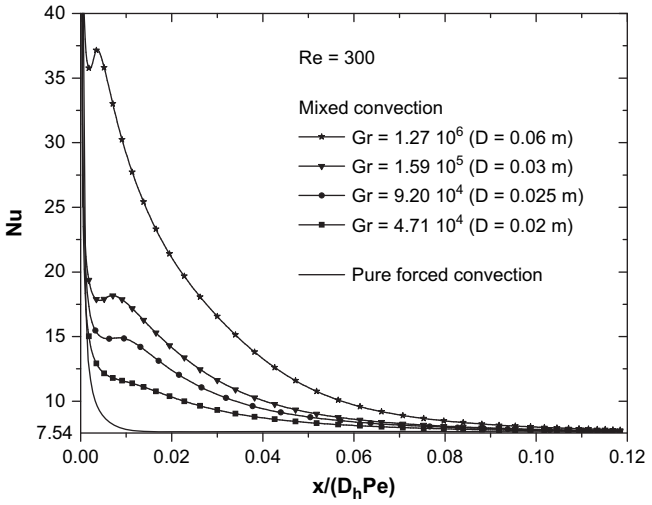

Fig. 7. Streamwise variation of the local bulk Nusselt number at the walls, Re = 300, $A = 50$.

dimensional centreline and bulk temperatures for the Grashof numbers (or D) shown in Fig. 2 shows the same sharp increase in the channel entrance (not shown here for the sake of brevity) as those presented in Fig. 6, the curves superposing perfectly for $D \geq 0.03$ m while only small differences appear for $D = 0.02$ m. The heat is thus mainly transferred to the fluid in the channel entrance. In the case of uniform heat flux, there exists a constant temperature difference between the fluid bulk temperature and the wall temperature in the fully developed region, thus maintaining the reversal flow all along the heated region of the duct and slightly beyond if an adiabatic section follows the heated region. In the case of isothermal channel walls, the recirculation cells are promoted by the large temperature difference between the walls, and the bulk temperature that exists at the channel entrance which generate a large buoyancy force. But this buoyancy force quickly weakens due to the sharp increase of the bulk temperature and thus of the decrease in the temperature difference. This explains why a fully developed flow region with bidirectional flow cannot be found in the case of isothermal boundary conditions, recirculation cells always being of limited length.

Figs. 4–6 also show the effect of two different inlet velocity boundary conditions: a uniform profile corresponding to a well-rounded contraction section (full lines in Figs. 4–6) and a parabolic profile corresponding to fully developed flow (symbols in Figs. 4–6) with uniform inlet fluid temperature, T_0. Surprisingly, as can be seen in these figures, the influence of these two inlet boundary conditions is very weak even if there is no flow reversal (Fig. 5, $D = 0.02$ m). Marked differences can obviously be observed at the channel entrance for the centreline velocity (Fig. 5), due to existence of maximums for parabolic velocity profiles. However, the curves become indistinguishable very quickly. The largest difference can be seen on the temperature profile at the channel entrance (Fig. 4b), though not exceeding a few percent. This seems to be in sharp contrast with the results of Zeldin and Schmidt [4] in a vertical tube with uniform wall temperature, who numerically found great differences in the trend of centreline velocity for both cases. However, the pipe entrance was enlarged on their diagrams with the use of a logarithmic abscissa. Looking carefully at their results, large differences between these two cases arise in less than the first 5–10 percent of the heated pipe: the "apparent" differences are smaller than they appear at first glance.

Finally, Fig. 7 presents the evolution of the local bulk Nusselt number for the various cases studied in Figs. 2 and 3, with fixed

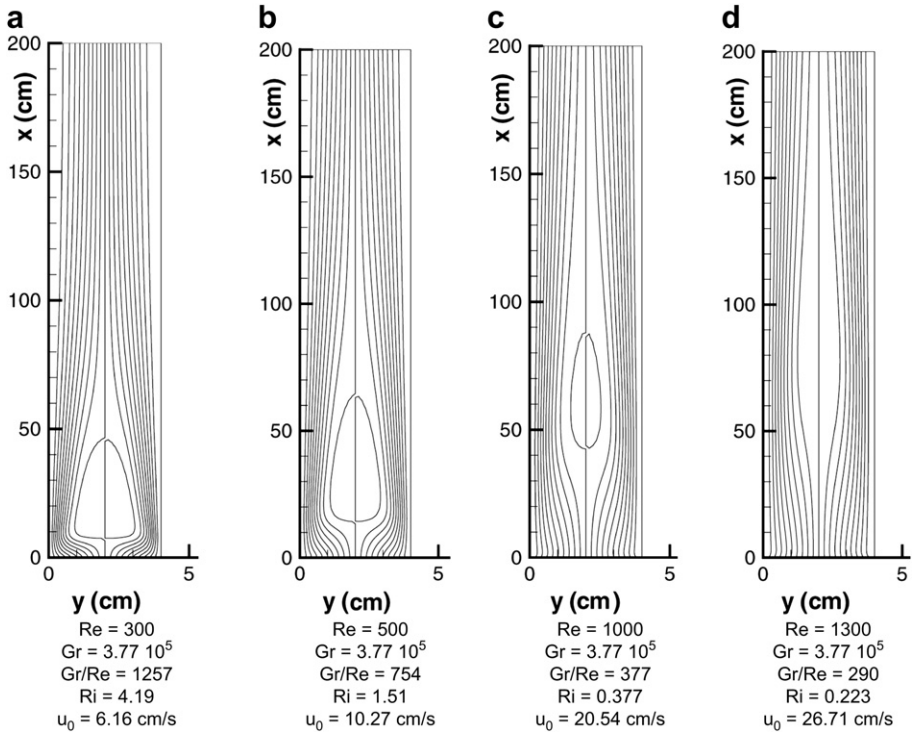

Fig. 8. Streamlines for various Reynolds numbers at a fixed width of the channel, $D = 0.04$ m. Note that the scale of the transverse direction is 10 times the scale of the axial direction. (Isolines: from 0 to 1 by 0.05 step). a) Re = 300, $Gr = 3.77 \times 10^5$, Gr/Re = 1257, Ri = 4.19, $u_0 = 6.16$ cm s^{-1}. b) Re = 500, $Gr = 3.77 \times 10^5$, Gr/Re = 754, Ri = 1.51, $u_0 = 10.27$ cm s^{-1}. c) Re = 1000, $Gr = 3.77 \times 10^5$, Gr/Re = 377, Ri = 0.377, $u_0 = 20.54$ cm s^{-1}. d) Re = 1300, $Gr = 3.77 \times 10^5$, Gr/Re = 290, Ri = 0.223, $u_0 = 26.71$ cm s^{-1}.

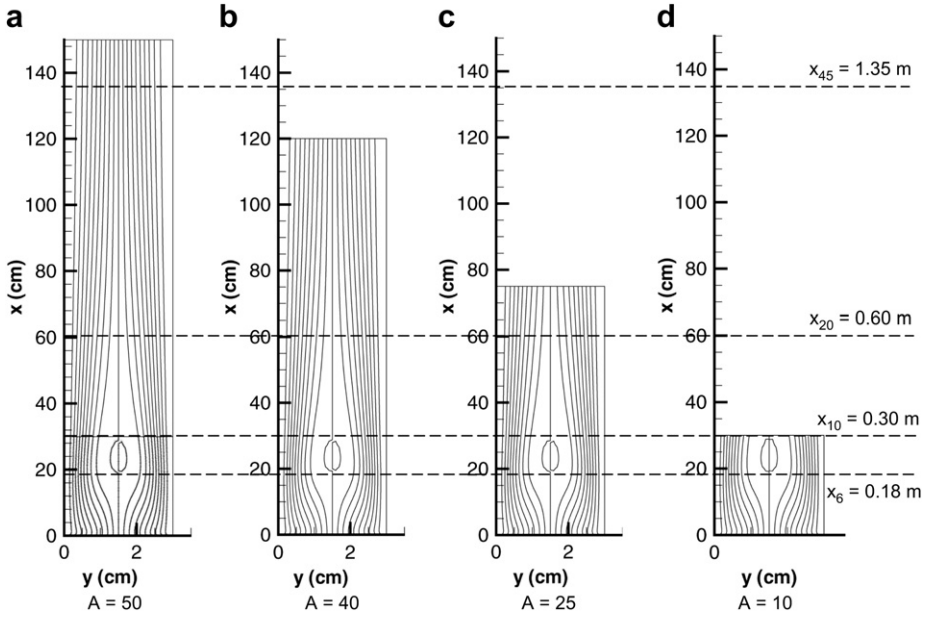

Fig. 9. Streamlines for various aspect ratios at fixed Reynolds number and width of the channel: Re = 500, Gr = 1.59×10^5 ($D = 0.03$ m), Gr/Re = 318, Ri = 0.64. *Note that the scale of the transverse direction is 10 times the scale of the axial direction. (Isolines: from 0 to 1 by 0.05 step).* a) $A = 50$, b) $A = 40$, c) $A = 25$, d) $A = 10$.

Reynolds number of 300 and various Grashof numbers. The non-dimensional abscissa $x/(D_h\,\mathrm{Pe})$ is in fact the inverse of the Graetz number and allows a single curve showing a monotonic exponential decrease to be drawn for the case of pure forced convection (*i.e.*, $\mathrm{Gr/Re} = 0$) whatever the Reynolds number. In this limiting case of pure forced convection, the buoyancy force is uniformly distributed across the channel. Fig. 7 shows that the natural convection always increases the heat transfer and its efficiency increases when the channel width increases. This is due to the slowing down of the flow when the Grashof number is increased (remember that Gr is increased through the increase of the channel width D; see also the values of u_0, Fig. 2) causing the extension of the reversed flow in the transverse and in the axial directions. This in turn, accelerates the fluid flow along the wall over a longer distance and thus increases the heat transfer efficiency. Furthermore, the Nusselt curves for the highest Grashof numbers, for which recirculation cells occur, present a maximum that corresponds to the flow reversal departure. It should be noticed that the location of these maxima is the same as the location of the maxima of the product $f\,\mathrm{Re}$ (not shown here for the sake of brevity).

3.2. Influence of the Reynolds number

Fig. 8 shows the effect of Re (or equivalently, of Pe, since Pr is fixed in the present study). This figure clearly shows that the locations, sizes and shapes of the flow recirculation regions appearing at the centre of the channel strongly depend on the Reynolds number. The flow recirculation regions are always initially located at the

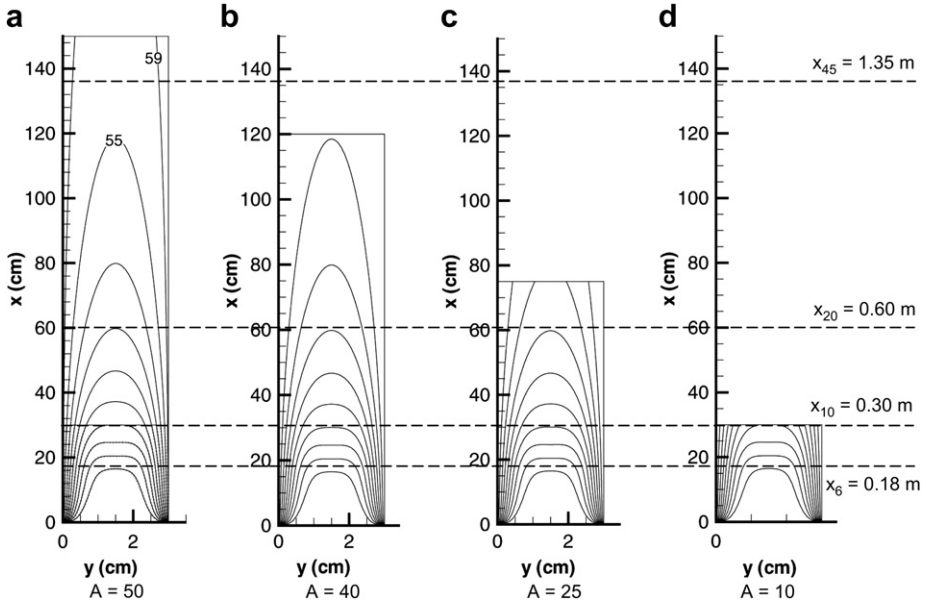

Fig. 10. Thermal fields for various aspect ratios at fixed Reynolds number and width of the channel, Re = 500, $D = 0.03$ m *(Isolines: from 10 °C (inlet) to 60 °C (walls) by 5 °C step + 59 °C).* a) $A = 50$, b) $A = 40$, c) $A = 25$, d) $A = 10$.

entrance of the channel (Fig. 8a). The width of the recirculation cells diminishes as the Reynolds number increases but they disappear before reaching the channel exit. In this case, the channel width, and hence the Grashof number is constant. As can be seen in Fig. 6, the buoyancy force is strongest at the channel entrance where the temperature difference between the fluid and the walls is large. Increasing the Reynolds number increases the inertia force which pushes away the recirculation cells in regions of low temperature difference where the buoyancy force weakens (Fig. 8c, Re = 1000) and thus the reversal flow disappears (Fig. 8d, Re = 1300). Flow inversion is detected near dimensionless locations $0.003 \leq x/(D_h \mathrm{Re}) \leq 0.007$ for all of the current computational data. The lowest location (0.003) is found for the highest Grashof number, very close to the channel entrance, while the highest location (0.007) is reached for the highest Reynolds number just before the recirculation has disappeared. The highest location is also the critical location, the location at which the reversal flows occur. This is substantially lower to what was determined in a circular tube (around 0.016 [11]) by solving the parabolic equations.

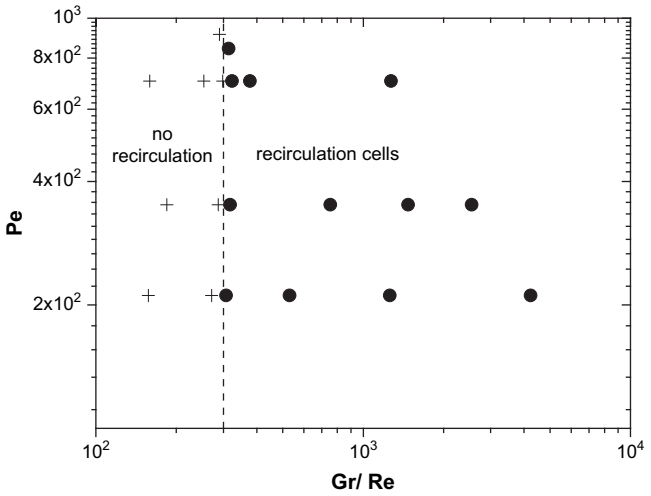

Fig. 12. Regime of reversed flow occurrence for air (+: without recirculation, •: with recirculation cells).

3.3. Influence of the channel aspect ratio

Streamlines and isothermal patterns obtained from the numerical simulations at Re = 300 for various aspect ratios are presented in Figs. 9 and 10, respectively. The channel width is kept constant and equal to $D = 0.03$ m. The Grashof number is thus equal to 1.59×10^5 for all of these runs. Surprisingly, the shape and size of the recirculation region at the centre of the channel entrance is not affected by the channel length even for aspect ratios as small as 10 (Fig. 9d). Contour plots of the stream function and temperature distributions for $A = 50$ and $A = 10$ superpose so well that they are indistinguishable in Figs. 9a and 10a respectively. This also demonstrated that the boundary conditions generally used at the outlet, *i.e.*, zero streamwise gradients (Eq. (7)), which are not always physically realistic when the fluid flow is not fully developed on reaching the outlet (see Fig. 9d for example), are nevertheless well suited as they did not numerically affects the flow too much.

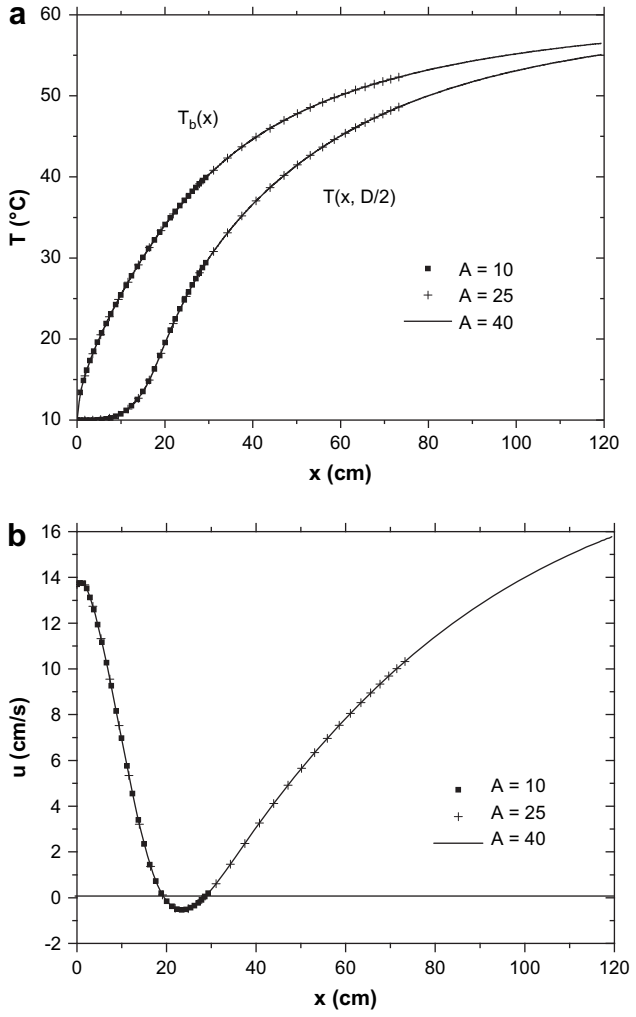

Fig. 11. Streamwise variation of the centreline and bulk temperature (a) and of the axial velocity (b) for various aspect ratios: Re = 500, Gr = 1.59×10^5 ($D = 0.03$ m), Gr/Re = 318, Ri = 0.64.

These findings are well exemplified in Fig. 11a and b, presenting respectively the streamwise variation of the centreline temperature and bulk temperature and the axial velocity. As can be seen, these profiles superpose perfectly for the three aspect ratios considered. It should be noted that the reversed flows presented in Fig. 2 for an aspect ratio of 50 are also obtained for a shorter channel length of 1.00 m corresponding to an aspect ratio of 40 (Fig. 2b), 33.33 (Fig. 2c) and 16.66 (Fig. 2d), the streamlines being once again indistinguishable. In the case of Fig. 8, for an aspect ratio of 25 instead of 50, the streamlines are also indistinguishable.

Fig. 12 shows the regime of reversed flow occurrence as a function of Pe (or Re since the calculations are only for Pr = 0.7) and Gr/Re. The cross symbols are for flow without recirculation cells while full black circles are for flow with recirculation cells. The dashed line indicating the separation between these two regimes is almost vertical, independent of the Péclet number, at Gr/Re ≈ 300. The lowest value of the Gr/Re ratio at which reversed flow was numerically found by Ingham et al. [20] by the use of an improved marching technique is 350, positioned slightly inside the reversed flow region. It is found here that the line demarcating the flow reversal is independent of the Reynolds (Péclet) number.

4. Conclusions

Laminar mixed convection of air in a vertical heated channel was numerically investigated in the case of buoyancy-assisted flow situations for both high Grashof and Reynolds numbers. Up to now, apart from a few isolated investigations, no systematic study of the occurrence of recirculation cells in the developing flow region in

symmetrically heated vertical channel at constant temperature has been performed. Most have failed to evidence such recirculation cells [18,19,22], except in [20]. The overall focus of this study was to obtain quantitative information on the effects of recirculation cells associated with flow reversal on hydrodynamic and heat transfer in vertical parallel-plate channels of finite length. The fundamental role of the isothermal boundary conditions of the channel walls in the occurrence and behaviour of flow reversal has been emphasized in the present paper, and a parametric study has been carried out.

In the case of isoflux conditions, the reversed circulation is able to extend all along the heated channel due to the constant difference between the wall temperature and the bulk temperature, and a fully developed flow with bidirectional flow can appear. In the case of isothermal boundary conditions, the increase of the fluid temperature is so large in the channel entrance that the reversal flow can only occur in this developing flow region. On the other hand, the buoyancy force becomes too small to sustain recirculation flow farther downstream in the second half of a long enough channel, *i.e.,* the fully developed flow region. Moreover, the regime of flow reversal is independent of the Péclet number for $Pe > 200$ and occurs for $Gr/Re \geq 300$. The critical location at which recirculation cells occur has been found near the channel entrance at $[x/(D_h Re)]_{crit.} \approx 0.007$, substantially lower to what was determined in a circular tube (around 0.016).

It has been numerically demonstrated that it is the sharp increase in the fluid temperature at the channel entrance which produces flow reversal. Increasing the Reynolds number increases the inertia forces: that push the recirculation cells into regions where the buoyancy forces weaken. The reversed flow disappears thus before reaching the exit of the channel. It has also been shown that the channel length has no influence on the shape and size of the recirculation cells provided the channel is long enough ($H/D \geq 10$).

Looking at the bulk Nusselt number, it has been shown that taking into account the effect of buoyancy leads to large increases in heat transfer compared to pure forced convection. It has also been demonstrated that the shape of the inlet velocity profile has a weak effect on the results.

Acknowledgements

The authors acknowledge the help of H. Sun for the implementation of the IDEAL algorithm. The authors also wish to thank the French National Institute for Advances in Scientific Computations (IDRIS) for computational support of this project through grant No. 07 1265. Finally, the authors wish to thank the referees for their valuable comments.

References

[1] J.D. Jackson, M.A. Cotton, B.P. Axcell, Study of mixed convection in vertical tubes, Int. J. Heat Fluid Flow 10 (1) (1989) 2–15.
[2] T.J. Hanratty, E.M. Rosen, R.L. Kabel, Effect of heat transfer on flow field at low Reynolds numbers in vertical tubes, Ind. Eng. Chem. 50 (5) (1958) 815–820.
[3] G.F. Scheele, T.J. Hanratty, Effect of natural convection on stability of flow in a vertical pipe, J. Fluid Mech. 14 (1962) 244–256.
[4] B. Zeldin, F.W. Schmidt, Developing flow with combined forced-free convection in an isothermal vertical tube, J. Heat Transfer 94 (1972) 211–223.
[5] L.S. Yao, Is a fully developed and non-isothermal flow possible in a vertical pipe? Int. J. Heat Mass Transfer 30 (4) (1987) 707–716.
[6] B.R. Morton, D.B. Ingham, D.J. Keen, P.J. Heggs, Recirculating combined in laminar pipe flow, J. Heat Transfer 111 (1989) 106–113.
[7] D.B. Ingham, D.J. Keen, P.J. Heggs, B.R. Morton, Recirculating pipe flows, J. Fluid Mech. 213 (1990) 443–464.
[8] M.A. Bernier, B.R. Baliga, Visualization of upward mixed-convection flows in vertical pipes using a thin semi-transparent gold-film heater and dye Injection, Int. J. Heat Fluid Flow 13 (3) (1992) 241–249.
[9] M.A. Bernier, B.R. Baliga, Conjugate conduction and laminar mixed convection in vertical pipes for upward flow and uniform wall heat flux, Num. Heat Transfer 21A (1992) 313–332.
[10] M. Wang, T. Tsuji, Y. Nagano, Mixed convection with flow reversal in the thermal entrance region of horizontal and vertical pipes, Int. J. Heat Mass Transfer 37 (15) (1994) 2305–2319.
[11] A. Moutsoglou, Y.D. Kwon, Laminar mixed convection flow in a vertical tube, J. Thermophys. Heat Transfer 7 (2) (1993) 361–368.
[12] H. Nesreddine, N. Galanis, C.T. Nguyen, Effects of axial diffusion on laminar heat transfer with low Péclet numbers in the entrance region of thin vertical tubes, Num. Heat Transfer 33 (1998) 247–266.
[13] M. Zghal, N. Galanis, C.T. Nguyen, Developing mixed convection with aiding buoyancy in vertical tubes: a numerical investigation of different flow regime, Int. J. Therm. Sci. 40 (2001) 816–824.
[14] W. Aung, G. Worku, Theory of fully developed, combined convection including flow reversal, J. Heat Transfer 108 (1986) 485–488.
[15] C.-H. Cheng, H.-S. Kou, W.-H. Huang, Flow reversal and heat transfer of fully developed mixed convection in vertical channels, J. Thermophys. 4 (3) (1990) 375–383.
[16] Y.-C. Chen, J.N. Chung, The linear stability of mixed convection in a vertical channel flow, J. Fluid Mech. 325 (1996) 29–51.
[17] Ch Guillet, Th Mare, C.T. Nguyen, Application of a non-linear local analysis method for the problem of mixed convection instability, Int. J. Non-Linear Mech. 42 (2007) 981–988.
[18] S. Habchi, S. Acharya, Laminar mixed convection in a symmetrically or asymmetrically heated vertical channel, Num. Heat Transfer 9 (1986) 605–618.
[19] W. Aung, G. Worku, Developing flow and flow reversal in a vertical channel with asymmetric wall temperatures, J. Heat Transfer 108 (1986) 229–304.
[20] D.B. Ingham, D.J. Keen, P.J. Heggs, Two dimensional combined convection in vertical parallel plate duct, including situations of reverse flows, Int. J. Num. Methods Eng. 26 (7) (1988) 1645–1664.
[21] D.B. Ingham, D.J. Keen, P.J. Heggs, Flows in vertical channels with asymmetric wall temperatures including situations where reverse flows occur, J. Heat Transfer 110 (1988) 910–917.
[22] Y. Azizi, B. Benhamou, N. Galanis, M. El-Ganaoui, Buoyancy effects on upward and downward laminar mixed convection heat and mass transfer in a vertical channel, Int. J. Num. Methods Heat Fluid Flow 17 (3) (2007) 333–353.
[23] C.-H. Cheng, C.-J. Weng, W. Aung, Buoyancy assisted flow reversal and convective heat transfer in entrance region of a vertical rectangular duct, Int. J. Heat Fluid Flow 21 (2000) 403–411.
[24] S.V. Patankar, Numerical heat transfer and fluid flow, Washington, D.C., 1980.
[25] D.L. Sun, Z.G. Qu, Y.L. He, W.Q. Tao, An efficient segregated algorithm for incompressible fluid flow and heat transfer problems- IDEAL (Inner Doubly iterative Efficient Algorithm for Linked equations) Part I: mathematical formulation and solution procedure, Num. Heat Transfer 53B (2008) 1–17.
[26] D.L. Sun, Z.G. Qu, Y.L. He, W.Q. Tao, An efficient segregated algorithm for incompressible fluid flow and heat transfer problems- IDEAL (Inner Doubly iterative Efficient Algorithm for Linked equations) Part II: application examples, Num. Heat Transfer 53B (2008) 18–38.
[27] G. Desrayaud, G. Lauriat, A numerical study of natural convection in partially open enclosures with a conducting side-wall, J. Heat Transfer 126 (2004) 76–83.
[28] Fluent 6, User's Guide, Fluent, 2006.
[29] N. Laaroussi, G. Lauriat, G. Desrayaud, Effects of variable density for film evaporation on laminar mixed convection in a vertical channel, Int. J. Heat Mass Transfer 52 (2009) 151–164.